Eur Radiol (2005) 15: 1734–1744
DOI 10.1007/s00330-005-2698-9

UROGENITAL

Emilio Quaia
Rossana Bussani
Maria Cova
Roberto Pozzi Mucelli

Radiologic–pathologic correlations of intratumoral tissue components in the most common solid and cystic renal tumors. Pictorial review

Received: 30 August 2004
Revised: 12 January 2005
Accepted: 20 January 2005
Published online: 8 March 2005

Presented as educational exhibit in EPOS 2004 and awarded by Cum Laude at ECR 2004

E. Quaia (✉) · M. Cova
Department of Radiology,
Cattinara Hospital,
University of Trieste,
Strada di Fiume 447,
34149 Trieste, Italy
e-mail: equaia@yahoo.com
Tel.: +39-40-3994372
Fax: +39-40-3994500

R. Bussani
Department of Pathology,
University of Trieste,
Trieste, Italy

R. P. Mucelli
Department of Radiology,
Hospital G.B. Rossi,
University of Verona,
Piazza L.A. Scuro 10, 37134,
Verona, Italy

Abstract This paper describes the correlation between US-CT images and pathologic findings in the most common solid and cystic renal tumors, to better differentiate malignant and benign renal masses. Several intratumoral tissue components present correlation with US-CT images. Macroscopic components, corresponding to necrotic, hemorrhagic and cystic changes, are identified by visual analysis of the gross specimen, while microscopic components are identified by histopathologic analysis. Microscopic components are classified as cellular [(1) high cellularity with poor extracellular stroma, ±high nucleus–cytoplasm ratio±high uniformity in tumoral cells dimensions; (2) low cellularity with large extracellular stroma±low nucleus–cytoplasm ratio± low uniformity in tumoral cells dimensions], stromal [(1) fibrotic; (2) fibrovascular; (3) fibromyxoid], vascular related to neoangiogenesis, necrotic [(1) coagulative; (2) colliquative; (3) hemorrhagic], calcific, and adipose.

Keywords Renal tumors · US · CT · Radiologic–pathologic correlations

Introduction

Malignant renal tumors Malignant renal cell carcinoma (RCC) presents different histopathologic subtypes: (1) clear cell (70–80%), (2) papillary cell (10–15%), (3) granular cell (5%), (4) chromophobe cell (5%) which generally present an expansile growth pattern, and (5) sarcomatoid cell (1–2%), (6) collecting duct carcinoma and (7) medullary carcinoma (1–2%) which generally present an infiltrative growth pattern [1–6].

Clear cell RCC is the most commonly found renal tumor, affecting approximately 12,500 adults per year in the USA [7]. On gross specimen, the clear cell type RCC presents a yellow-golden appearance, due to the rich lipid content of its cells which are markedly similar to that of the proximal convoluted tubules. Areas of necrosis, cystic degeneration,

hemorrhage and calcification are seen. Distinct areas of fat may be present in RCC. In RCC the fat component may be produced by lipid-producing necrosis in large RCC, by the intratumoral bone metaplasia with fatty marrow elements and calcification within a small RCC, or by the entrapment of perirenal or sinus fat by large RCC [8]. Cystic areas may be generally present so that the tumor has a frank cystic appearance. The cells are typically rich in glycogen, interspersed abundantly with thin-walled blood vessels and, when stained appear clear or lucent [9, 10]. Well-differentiated tumors usually have a uniform pattern, predominantly of the alveolar or acinar variety, while solid sheets of neoplastic cells are characteristic of poorly differentiated neoplasms.

Papillary (chromophil) RCC presents a variable cut surface, from light gray to golden yellow [11, 12] depending on the amount of lipid-laden macrophages in the papillae. The color depends on the amount of lipid-laden macrophages in the stroma [6]. Intralesional hemorrhage and necrosis are frequently observed (50–67% of cases). Fibrovascular stalks with frondlike projections are characteristic of papillary tumors. These lesions are villous, with vascularized stalks lined with characteristic densely stained cells and foamy histiocytes [8]. Type A—type 2 (75% of cases) is a more aggressive form of cancer than type B—type 1 and appears as a single mass, usually bulky, either solid and cystic in a ratio of approximately 2:1. Type B (25% of cases) is found in hereditary papillary RCC, is associated with a better long-term prognosis than type A and consists of multicentric lesions, often bilateral (67%) [6].

Granular cell type RCC resembles clear cell type RCC but necrosis and hemorrhage are even more likely to be present. Predominant granular RCCs are most often single tumors with a male predominance (2:1). The cut surface of this tumor is brown because of the high lipochrome phospholipid content of the numerous cytoplasmatic organelles. Granular cells are usually intensely eosinophilic and contain little glycogen and lipid. Mixed tumors consisting of clear and granular cells also occur.

Chromophobic cell type RCC is relatively infrequent (<5%). There is evidence that the tumor arises from the intercalated cells of the collecting ducts. These tumors tend to be large, from 2 to 22 cm in the greatest dimension, and are well circumscribed and solitary, with a gray to brown appearance and typically lacking hemorrhage and necrosis [13]. Chromophobe carcinomas contain poorly staining cells with a reticular cytoplasm characterized by a perinuclear halo and peripheral cytoplasm rich in mitochondria [8, 14].

Sarcomatoid type RCC is a particularly poorly differentiated variant comprising about 1% of cases. This tumor, which can be considered as a poorly differentiated or undifferentiated variant of any mentioned RCC subtype, is usually large with a gray appearance due to fibrosis without hemorrhage and necrosis when the sarcomatoid portion predominates and a heterogeneous appearance with areas of necrosis and hemorrhage when the carcinomatous portion predominates.

Collecting duct carcinoma, known also as Bellini duct RCC, is a rare tumor representing less than 1% of primary malignant renal parenchymal epithelial neoplasms [6]. This variant seems to originate in the medulla and has predominately a tubular configuration. A typical infiltrative pattern, with preservation of the reniform shape, is the most common tumoral growth. Hemorrhage and necrosis are not typically present. Lymph node metastases may be expected and extension into the renal vein does not occur [15].

Benign renal tumors Benign renal parenchyma tumors are: (1) angiomyolipoma, and (2) oncocytoma.

Angiomyolipoma is a hamartoma [16] of the kidney that contains vascular, lipomatous, and myeloid elements [17]. It is an uncommon lesion with a prevalence from 0.3 to 3% and occurs more commonly in women than men [18, 19]. Angiomyolipomas are rare in children as isolated lesions, but are found in up to 80% of children with tuberous sclerosis, then usually being bilateral, small and multifocal [20]. The tumor appears usually as an expansive unifocal large mass which is yellowish on section when the fat component is prevalent, white if the muscular component is prevalent or red when the vascular component is prevalent which may present a hemorrhagic pattern [19]. Angiomyolipoma rarely may become locally aggressive, with invasion into adjacent nodes or within the inferior vena cava [8].

Oncocytoma (2–3% of renal tumors) is characterized by large cells with small, uniform, round nuclei and an abundant eosinophilic cytoplasm. It appears brown on section for the lipocromic pigment of mitochondria with or without calcifications and, generally, without necrosis and hemorrhage and with a fibromyxoid stroma in the central scar [21]. Oncocytomas are tan-brown in color owing to their mitochondria-rich cytoplasm. Microscopically, oncocytomas are composed of large dense cells with abundant highly granular eosinophilic cytoplasm due to mitochondria and arranged in solid, tubular, or trabecular rests [8]. The cells are large (onco means large) in comparison with the other cell types. They commonly grow centrifugally from a central avascular scar. Calcifications may occur in the central scar. Although oncocytomas are considered to be benign, reports of recurrence and even metastases following resection of oncocytomas suggest that these neoplasms have the capability to become malignant since they can contain chromophobe cells [8].

Growth patterns in renal tumors visualized by imaging Ultrasound (US) and CT have the capability to depict tumoral morphology and margins determined by the expansile or infiltrating growth pattern towards the adjacent renal parenchyma. Cross-sectional imaging procedures differentiate expansile from infiltrative growth patterns through analysis of the parenchymal interface between the tumor

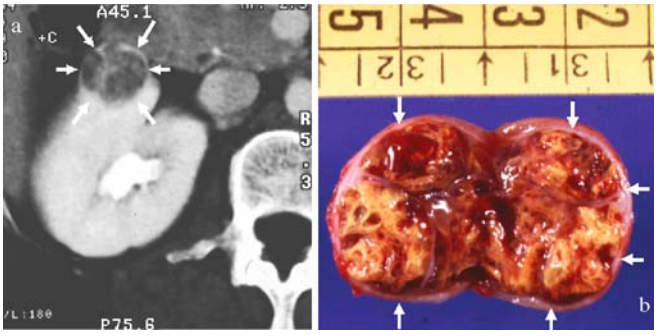

Fig. 1 Renal cell carcinoma, papillary cell type. Expansile growth pattern. **a** Contrast material-enhanced CT, excretory phase. A rounded renal mass appears well demarcated from the adjacent renal parenchyma by a thick tumoral pseudocapsule (*arrows*). **b** Gross specimen of the tumor which was surgically removed. Pseudocapsule is clearly evident (*arrows*)

and the kidney, the effect of the lesion on the collecting system and renal sinus, and the overall renal morphology.

(a) Expansile growth. The majority of renal tumors present an expansile growth pattern, characterized by radial tumor enlargement that impress adjacent renal parenchyma and forms spherical, often exophytic, lesions with well-defined margins [1]. The interface of the tumor and the adjacent kidney is usually well demarcated with a pushing margin [2]. The features of the expansile growth are spherical shape, focal bulging of the renal contour, displacement of normal parenchyma and collecting system elements, and pseudocapsule formation (Fig. 1). Pseudocapsule is composed by the thick renal parenchyma compressed by tumoral growth with increased deposition of fibrous tissue from ischemia, and necrosis of normal renal parenchyma [1]. It seems that pseudocapsule is a pathologic feature seen in the early stages, and it is considered as a sign for a localized intrarenal lesion confined to the renal capsule which can be treated by partial nephrectomy or, recently, by radiofrequency ablation [22]. Due to its fibrous component, tumoral pseudocapsule reveals a late enhancement after contrast agent injection at CT [1]. The most common renal tumors subtypes (clear cell and papillary cell type) typically appear as well defined masses and may present a pseudocapsule.

(b) Infiltrative growth. On the other hand, some renal tumors present an infiltrative growth pattern by using the normal renal parenchymal architecture for the interstitial growth, without a clear limit with the adjacent renal parenchyma, and usually with preservation of the reniform shape [1]. Infiltrative growth is a less frequent growth pattern of renal neoplasms but is nonetheless characteristic of certain renal tumors. The infiltrative processes more often encase rather than displace the intrarenal collecting system (Fig. 2). Replacement of the renal sinus fat is also characteristic. Specific entities that appear infiltrative include a variety of uncommon tumors such as renal medullary carcinoma and sarcomatoid tumor. Infiltrative growth may also be an atypical manifestation of more common neoplasms as clear cell type RCC.

Clinical series

During a period of 48 months, 51 solid renal tumor (42 malignant—29 clear cell, nine papillary cell, two granular cell, one chromophobic cell and one sarcomatoid cell type

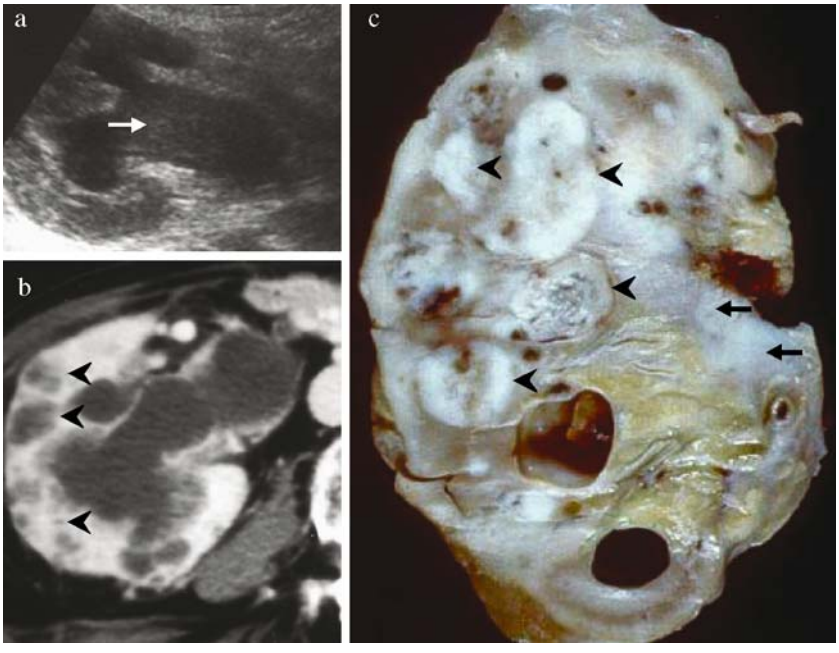

Fig. 2 RCC, sarcomatoid cell type. Infiltrative growth pattern. US (**a**) shows mild hydronephrosis with echoic content (*white arrow*). Contrast material-enhanced CT (**b**) confirms hydronephrosis and reveals also multiple round and hypodense parenchymal lesions (*arrowheads*) which were interpreted as renal abscesses. Diagnosis of pyonephrosis with renal parenchymal abscesses was proposed and nephrostomy was positioned. After necroscopy infiltrative tumor (*arrowheads*) was revealed at the gross specimen analysis (**c**). Infiltration of renal sinus (*arrowheads*) and pyeloureteral junction (*black arrows*) justified renal hydronephrosis. No pseudocapsule may be identified. Sarcomatoid cell type RCC was diagnosed at microscopic analysis

RCCs; and nine benign- five angiomyolipomas and four oncocytomas) and 15 cystic renal tumors (ten malignant—five clear cell and five papillary cell type; and five benign—multilocular cystic nephromas), from 2.8 to 8.3 cm in the largest diameter, identified in 66 patients (35 male and 31 female; mean age±SD, 60±11 years; age range 50–75 years) were surgically resected from 20 up to 40 days after detection, and retrospectively analysed.

In this study, each renal tumor was detected by conventional US (HDI 5000; Philips-ATL, Washington, USA) and then assessed by helical CT. Conventional US was performed by convex-array wideband transducer 2–5 MHz. Helical CT (Tomoscan AVE1, Philips, The Netherlands) was performed before and after intravenous bolus administration of 120–140 ml of non-ionic contrast material (iomeprol, Iomeron 300; Bracco, Milan, Italy) at a rate of 2 ml/s. Technical parameters were 3-mm collimation, 5-mm/s table movement and 3-mm reconstruction interval during cortico-medullary (25–80 s after contrast injection), nephrographic (85–120 s) and excretory (3–5 min) phase. Both US and CT images were available at a picture archiving and communication system that facilitated data analysis.

Firstly, the macroscopic appearance and each microscopic tumoral component were previously analysed by one pathologist (R.B.) with 20 years of experience in renal pathology. Secondly, macroscopic and microscopic features of each analysed renal tumor were correlated with US and CT images by three radiologists (E.Q., M.C., and R.P. M.), with respectively 10, 20 and 30 years of experience in renal tumors imaging, who worked in consensus. Those intratumoral tissue components which could be identified on US and CT images are presented.

Solid renal tumors

Multiple intratumoral tissue components were identified at macroscopic or histologic analysis of the specimen and revealed a correlation with imaging. The presence at the same time of different intratumoral microscopic tissue components mixed in different portions of the tumor determined heterogeneous appearance at US and CT.

Cellular components In solid renal tumors different microscopic components with a different grade of cellularity, amount of extracellular stroma, nucleus/cytoplasm ratio and uniformity in tumoral cells dimensions were identified. The most important element determining the tumoral appearance at imaging was the liquid content related to the grade of cellularity and the amount of the extracellular stroma. In renal tumors with high cellularity and poor extracellular stroma the liquid content of the tumor was low. The nucleus/cytoplasm ratio and the uniformity in tumoral cells dimensions were considered as adjunctive elements which may influence the tumoral liquid content. The high

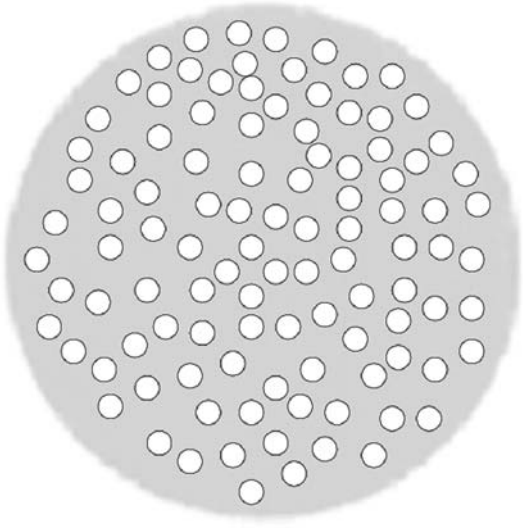

Fig. 3 High cellularity with poor extracellular stroma, ± high nucleus/cytoplasm ratio and high uniformity in tumoral cell dimension

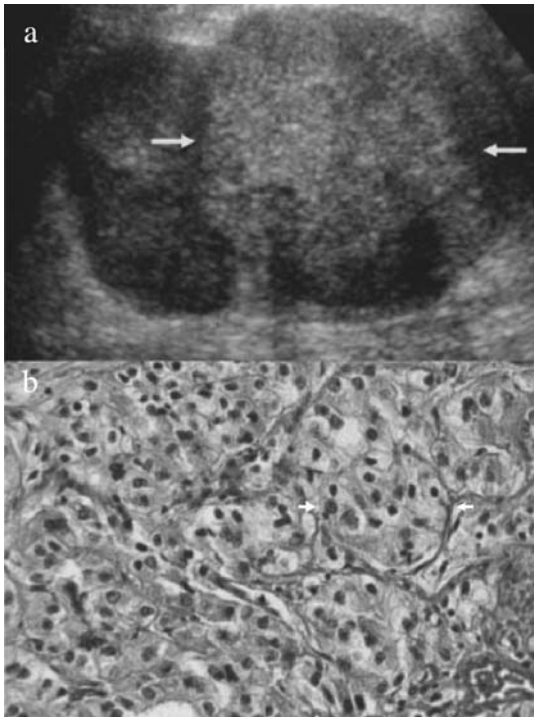

Fig. 4 RCC, clear cell type. High cellularity with poor extracellular stroma, high nucleus/cytoplasm ratio (*arrows*) and high uniformity in tumoral cells dimensions. **a** The tumor presents hyperechoic appearance (*arrows*) at US. **b** Hematoxylin and eosin, original magnification ×40. Microscopic examination shows cells with large nuclei and clear cytoplasm, arranged in an alveolar architectural pattern (*arrows*). The high number of tumoral cells with multiple acoustical interfaces, and the low water content both in the intracellular and extracellular compartments (**b**), determined the hyperechoic appearance at US

nucleus/cytoplasm ratio with large and central nuclei and poor cytoplasm was related to a low water content as the high uniformity in tumoral cells dimension.

(a) High cellularity with poor extracellular stroma±high nucleus/cytoplasm ratio±high uniformity in tumoral cells dimensions. This intratumoral microscopic component is represented in Fig. 3, and it was identified in 12/29 (41%) solid clear cell, in three of nine (33%) solid papillary cell, in granular cell and sarcomatoid cell type RCCs. Histologically evident nuclei and small cytoplasm amount are evident with a poorly represented extracellular stromal component. The appearance at imaging is determined by the high number of acoustical interfaces and by the relatively low amount of intracellular and extracellular liquid component. For these reasons, these tumors appeared hyperechoic at US (Fig. 4) and hyperdense at non-enhanced CT scan (Fig. 5). Contrast enhancement was low if compared to the adjacent renal parenchyma for the poor extracellular fibrovascular matrix with few vessels (Fig. 5).

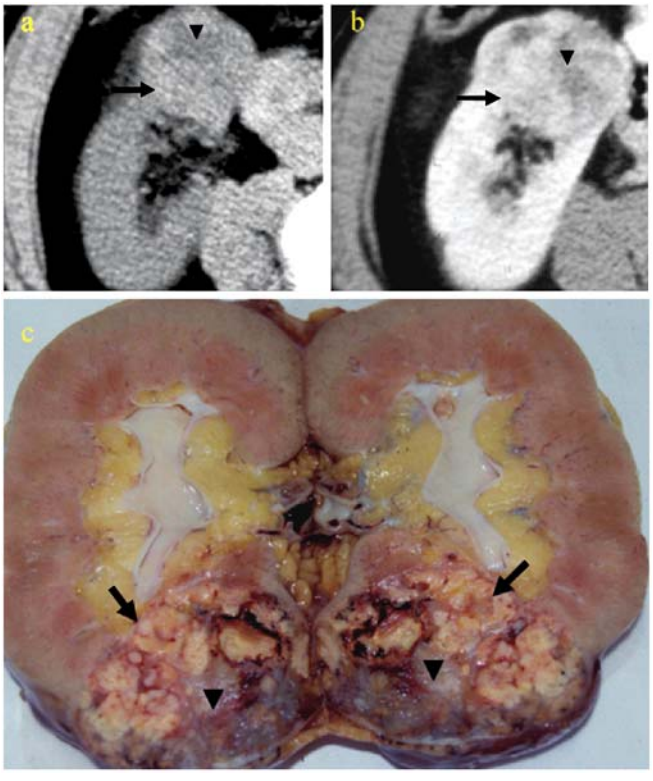

Fig. 5 RCC, clear cell type. High cellularity with poor extracellular stroma, high nucleus/cytoplasm ratio and high cellular uniformity and coagulative necrotic component. The tumor appears heterogeneous at non-enhanced CT (**a**) with a peripheral hyperdense component (*arrow*), corresponding to the cellular component with high cellularity, high nucleus/cytoplasm ratio and high cellular uniformity, and a central hypodense portion (*arrowhead*). At contrast material-enhanced CT (**b**) the peripheral solid viable component (*arrow*) reveals diffuse contrast enhancement while the central necrotic component (*arrowhead*) appears hypovascular. At the gross specimen analysis (**c**) a clear distinction between the solid peripheral viable component (*arrows*) and the central necrotic component (*arrowheads*) which presents hemorrhagic appearance

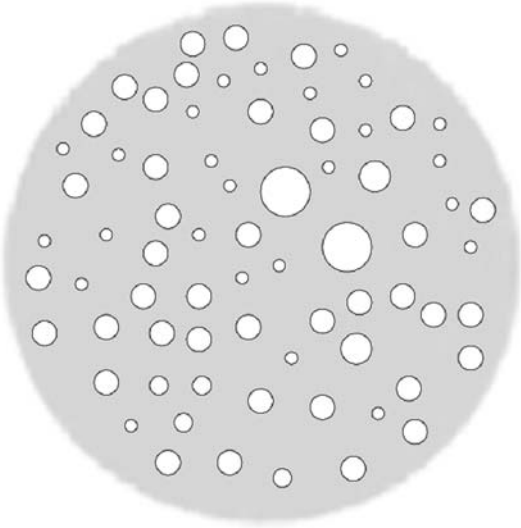

Fig. 6 Low cellularity with large extracellular stroma ±low nucleus/cytoplasm ratio and ±low uniformity in tumoral cell dimension

(b) Low cellularity with large extracellular stroma±low nucleus/cytoplasm ratio±low uniformity in tumoral cells dimension. This microscopic intratumoral tissue component is represented in Fig. 6, and it was identified in 17/29 (59%) solid clear cell, in six of nine (67%) solid papillary cell, and chromophobic cell type

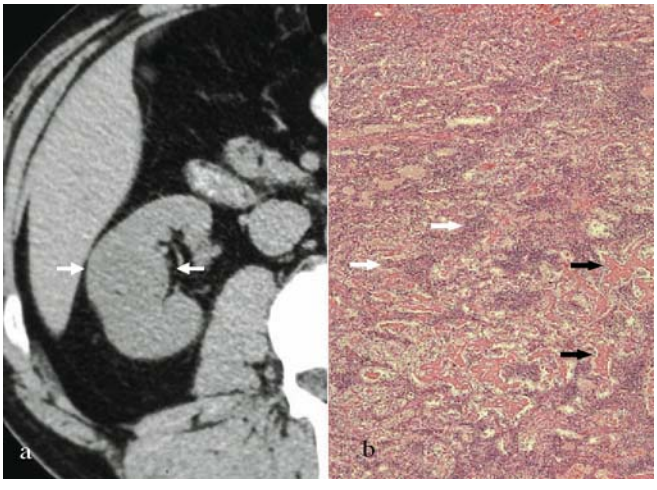

Fig. 7 RCC, clear cell type. Low cellularity with large extracellular stroma, low nucleus/cytoplasm ratio and low cellular uniformity. **a** Non-enhanced CT. The tumor presents isodense appearance to the adjacent kidney at non-enhanced CT. **b** Hematoxylin and eosin, original magnification ×20. The microscopic analysis reveals tumoral cells (*white arrows*) with a small nucleus (**b**), and large extracellular stroma with high amount of vessels (*black arrows*). The high liquid content both in the intracellular compartment and in the extracellular stroma determined the isodense appearance to the adjacent kidney at non-enhanced CT

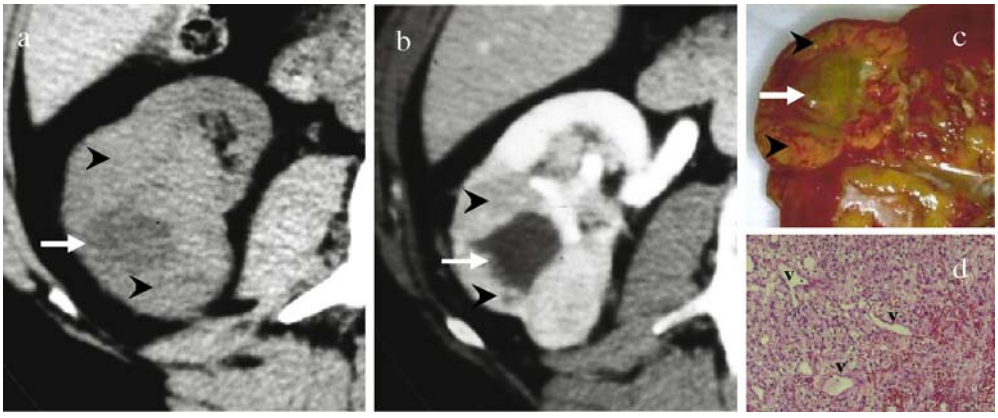

Fig. 8 RCC, clear cell type. Low cellularity with large extracellular stroma, low nucleus/cytoplasm ratio and low cellular uniformity. The peripheral tumoral portion appears isodense (*arrowheads*) to the adjacent renal parenchyma at non-enhanced CT (**a**). Diffuse contrast enhancement (*arrowheads*) is revealed at contrast material-enhanced CT (**b**) in the peripheral solid tumoral viable component (**c**). The central coagulative necrotic component (*arrow*) appears hypovascular at contrast material-enhanced CT (**b**), and it is confirmed at the gross specimen analysis (**c**) where it presents a yellowish appearance (*arrow*). Microscopic analysis (**d**), at hematoxylin and eosin staining; original magnification ×20 reveals a large vascular component (*v*) of the extracellular stroma which determined contrast enhancement in the viable tumoral component

RCCs. Histologically hyperchromic small nuclei and vacuolized cytoplasm are evident and large extracellular stromal component is observed. This component appeared heterogeneous at US and iso- or hypodense at non-enhanced CT (Fig. 7) due to the high intra- and extracellular liquid component. The diffuse contrast enhancement (Fig. 8) after contrast agent administration was due to the large fibrovascular extracellular component.

Stromal components This microscopic component also presents evidence at the gross specimen analysis, and it is always present in a solid renal tumor, even though it may be sometimes undetectable by imaging procedures for limited spatial and contrast resolution. In all types of stromal components iodinated contrast agents administration produces a lower enhancement that the adjacent renal viable tumor with hypovascular appearance (Fig. 9).

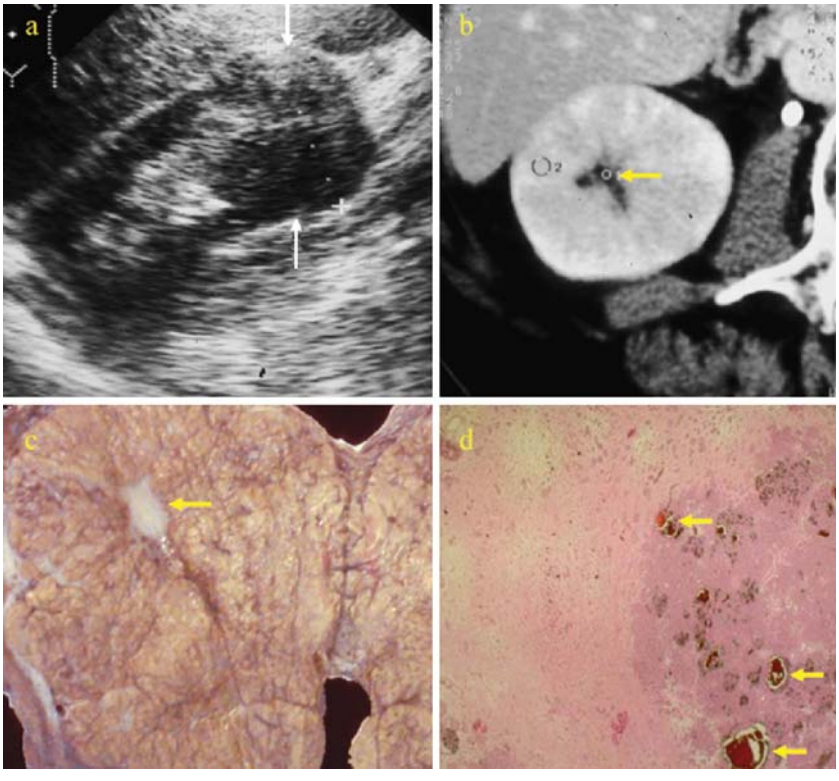

Fig. 9 Renal oncocytoma. Fibrovascular and fibromyxoid component. The tumor (*arrows*) appears heterogeneous at US (**a**) and revealed a central hypodense portion (*arrow*) at contrast material-enhanced CT (**b**). The resected tumor (**c**) reveals a central white scar (*arrow*) which revealed a uniform fibromyxoid appearance at the microscopic analysis (**d**; hematoxylin and eosin, original magnification ×40) with few vessels (*arrows*)

(a) Stromal fibrotic. It was identified in 3/29 (10.4%) solid clear cell RCCs. It appeared hyperechoic at US and isohypodense at non-enhanced CT if compared to the adjacent cellular tumoral components.
(b) Stromal fibrovascular. It was identified in solid papillary cell RCCs. Besides vessels, this component comprises inflammatory cells, necrosis and edema. The appearance was hypoechoic or isoechoic at US and hypodense at non-enhanced CT due to the low cellular component and to the large extracellular fibrovascular matrix.
(c) Stromal fibromyxoid. It was identified in four out of four (100%) renal oncocytomas. This is a variant of fibrovascular component and is characterized by the high liquid stromal component and by a variable vascular component (Fig. 9).

Vascular neoangiogenetic component Tumoral neoangiogenesis component determined contrast enhancement in the viable portion of all solid malignant tumors, and in the septal and peripheral nodular enhancement of cystic malignant renal tumors. This microscopic tissue components, corresponding to the process of new blood vessels formation, determines tumoral growth and metastases formation. Neoangiogenesis determines the grade of vascularization of renal tumors. It is generally observed in malignant renal tumors and may be exhaustively assessed only at the microscopic evaluation. Baseline color and power Doppler techniques are not effective in identifying this component, while microbubble-based or paramagnetic contrast agents, as well as molecular imaging techniques, are the most proper tools to identify neoangiogenesis [23, 24]. Dynamic contrast material-enhanced MR imaging can aid non-invasively the diagnosis of angiogenic activity by enabling the measurement of tumoral perfusion, increased microvessel permeability and blood volume [25]. Large-molecular contrast agents were experimentally proved to be particularly suitable to assess tumoral perfusion [26, 27].

Necrotic tumoral changes Areas of coagulative (yellowish) or hemorrhagic (red) necrosis were identified at the gross specimen analysis, and revealed also typical appearance at the microscopic analysis. The viable part of the neoplasm revealed enhancement at contrast material-enhanced CT while the necrotic and hemorrhagic components appeared hypovascular (Fig. 5). In all types of necrotic changes, contrast agent administration produces a lower enhancement that the adjacent renal viable tumor with a consequent hypovascular appearance.

(a) Coagulative necrotic change. It was identified in 20/29 (68%) solid clear cell, in two of nine (22%) solid papillary cell, and granular cell type and sarcomatoid cell type RCCs. It is the most common type of necrosis found in renal tumors. Cells are transformed in an acidophilic agglomerate from intracellular proteins output. It presents a yellowish gross appearance and may evolve towards colliquative necrosis or fibrosis. Coagulative necrotic change appeared hypoechoic at US and hypodense at non-enhanced CT (Fig. 8).
(b) Colliquative necrotic change. It was identified in 9/29 (31%) solid clear cell and in seven of nine (77%) papillary cell RCCs. It is determined by the activity of the intracellular enzymes when lytic phenomena predominate over intracellular proteins denaturation. Colliquative necrotic change appeared hypoechoic at US and markedly hypodense at non-enhanced and contrast material-enhanced CT [28] (Fig. 10).

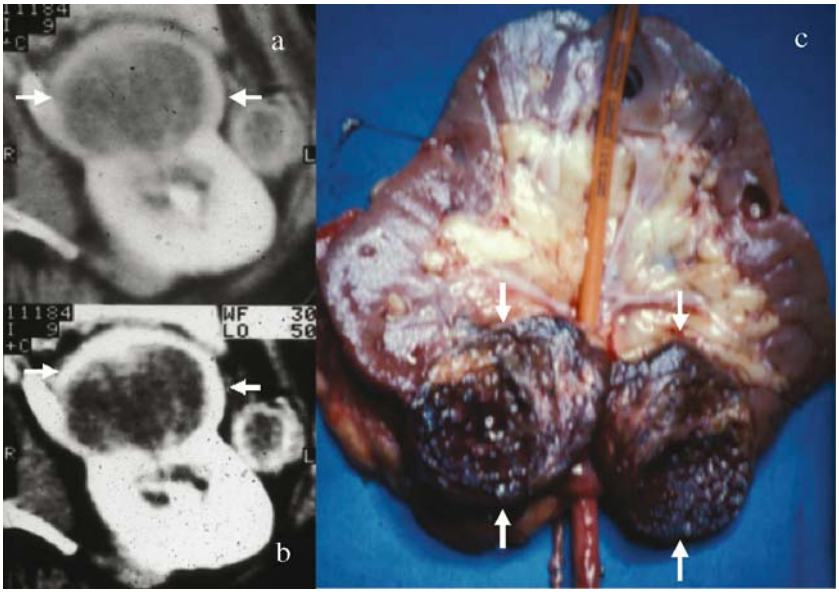

Fig. 10 Renal cell carcinoma, papillary cell type A. Colliquative necrotic change. Contrast material-enhanced CT, tubular (**a**) and excretory (**b**) phase shows a renal mass (*arrows*) with a peripheral thickened wall and a central hypodense core which corresponds to central colliquative necrosis (*arrows*) at the gross specimen analysis (**c**). The pattern may be defined a unilocular cystic pattern determined by extensive necrosis

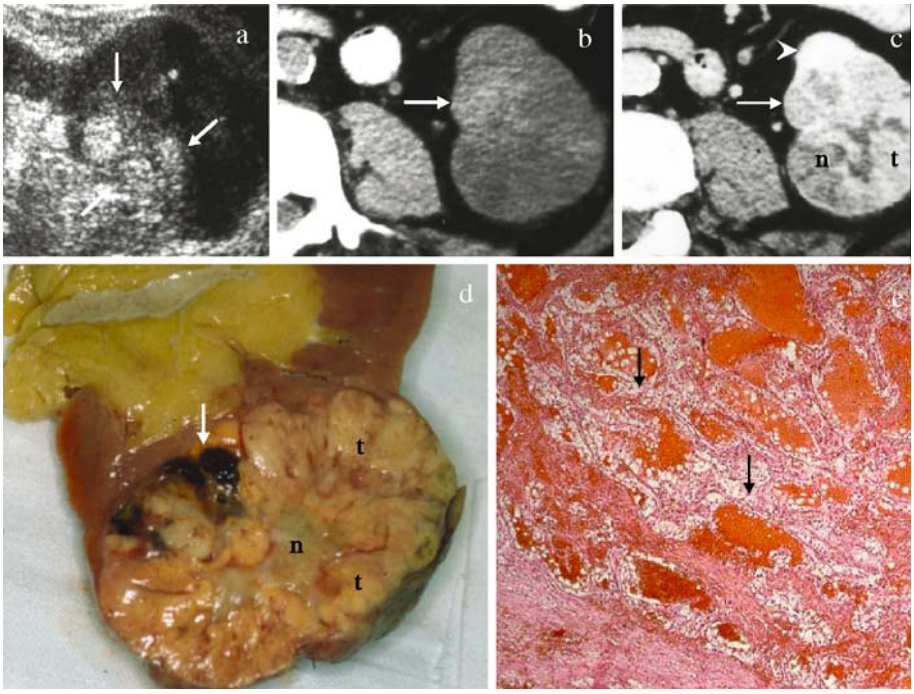

Fig. 11 RCC, clear cell type. Hemorrhagic necrotic change. The tumor appears heterogeneous at US (**a**) with a hyperechoic portion (*arrows*). The same region appears hyperdense (*arrow*) at non-enhanced CT (**b**) and hypovascular (*arrow*) at contrast material-enhanced CT (**c**) if compared with the adjacent renal parenchyma (*arrowhead*). The same region of the tumor reveals hemorrhagic necrotic change (*arrow*) at the gross specimen (**d**) which appears highly vascular and hemorrhagic with blood extravasation in the interstitial space at microscopic analysis (**e**; hematoxylin and eosin, original magnification ×40). The tumor appears very heterogeneous at contrast material-enhanced CT (**c**), due to the coexistence of the viable enhancing component (*t*) and of the hypovascular necrotic (*n*) component

(c) Haemorrhagic necrotic change. It was identified in 3/29 (10.5%) solid clear cell and in two out of two (100%) granular cell type RCCs. It is determined by blood extravasation through the necrotic microvessels walls and it may evolve towards fibrosis and calcification. The hemorrhagic necrotic change appeared hyperechoic at US and hyperdense at non-enhanced CT (Fig. 11).

Calcific component This was identified in 1/29 (3%) solid clear cell RCC. This microscopic tissue component may be associated with areas of fat. Calcifications may derive from degenerative or necrotic process. Calcifications appeared hyperechoic at US with a posterior acoustic shadowing and hyperdense at CT (Fig. 12).

Adipose component This component was identified in all angiomyolipomas. CT has an established role in detecting the fat component in renal tumors, particularly if non-enhanced thin sections (5 mm or less) are employed. Despite the detection of fat density (−10 to −100 HU) in a solid renal tumor, it is generally accepted that this lesion is likely to be an angiomyolipoma. In about 5% of angiomyolipomas the fat component may be identified only microscopically. Anyway, other solid renal tumors may present a fat component including RCCs, lipoma, liposar-

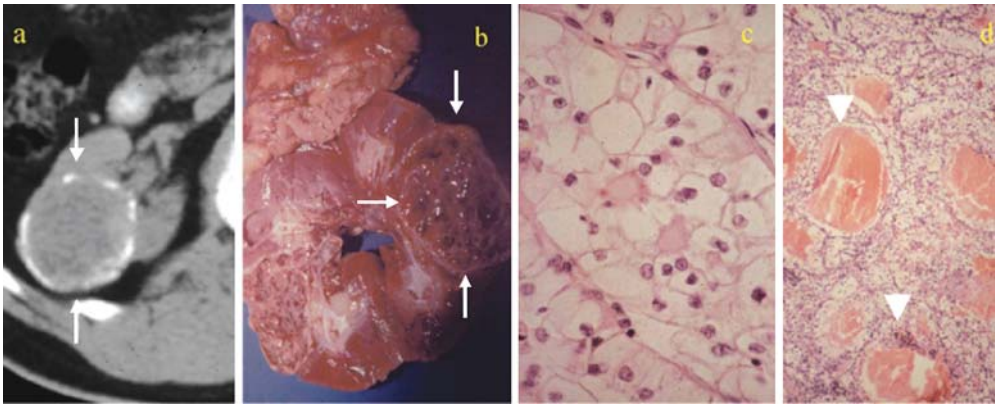

Fig. 12 RCC, clear cell type. Calcific component. The tumor (*arrows*) presents an hyperdense calcific peripheral component at non-enhanced CT, evident also at gross specimen analysis (**a**). The tumor (**b**) reveals the typical pattern of clear cell RCC (**c**; hematoxylin and eosin, original magnification ×50) at the microscopic analysis with some psammomatous corpora (*arrowheads*) expressing calcifications (**d**)

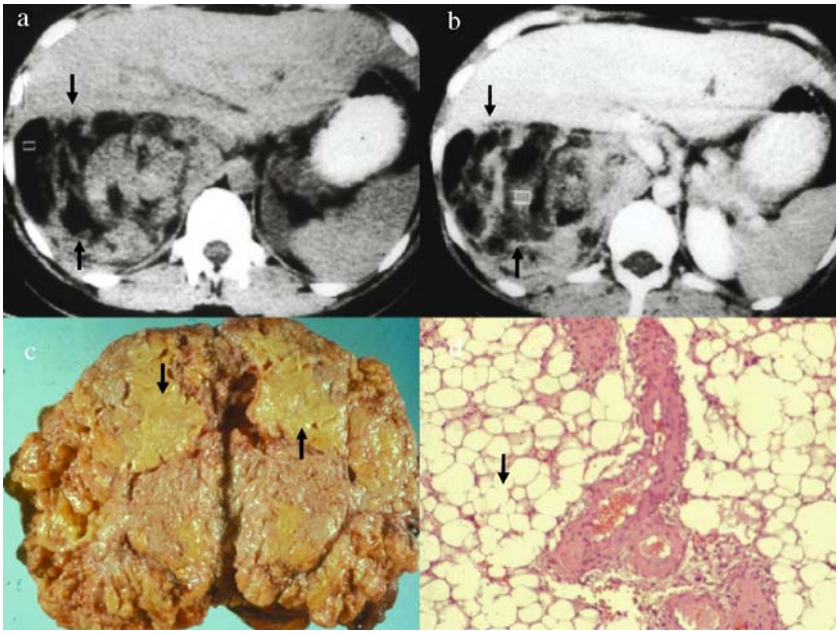

Fig. 13 Renal angiomyolipoma. tumor presents a fat component (*arrows*) hypodense at non-enhanced CT (**a**) and contrast material-enhanced CT (**b**). The gross specimen (**c**) reveals the adipose yellowish component (*arrows*). The microscopic specimen (**d**; hematoxylin and eosin, original magnification ×40) confirms the adipose component consisting of large foamy cells (*arrow*)

coma and oncocytoma [10, 29]. In a renal mass containing fat in addition to calcification, the possibility of RCC has to be seriously considered [29, 30]. MR chemical shift imaging is the most sensitive technique to identify fat component in renal tumors [31, 32]. The adipose component appeared hyperechoic at US and hypodense at non-enhanced CT (Fig. 13).

Cystic renal tumors

Cystic neoplasms may develop because of extensive tumor hemorrhage or necrosis, or they may have an inherently cystic growth pattern (renal cystadenocarcinoma). Cystic RCC includes any malignant neoplasm that present a fluid-filled mass. These neoplasms are often very difficult to

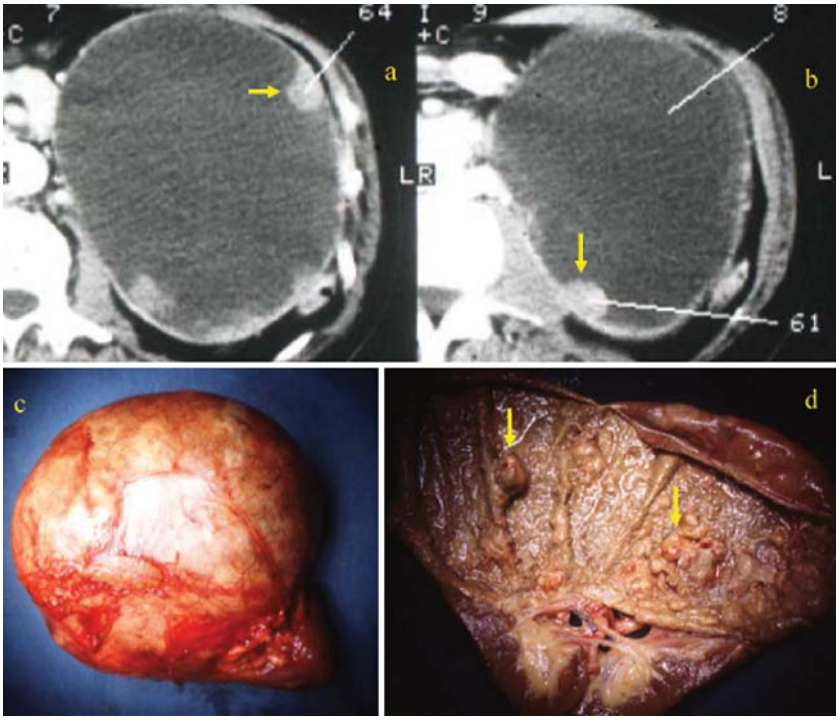

Fig. 14 RCC, papillary cell type A. Contrast material-enhanced CT (**a**, **b**) shows an unilocular cystic renal mass with mural nodules (*arrow*) and a thickened peripheral wall. The surgically removed renal mass (**c**) shows cystic pattern and mural nodules (*arrows*) also at the gross specimen analysis (**d**)

differentiate from complicated renal cysts and benign cystic neoplasm by imaging procedures alone. Renal cystic tumors are classified according to the CT appearance [33, 34]. Type 1=simple benign cysts; type 2=minimally complicated benign cyst; type 3=indeterminate cystic masses since their benignity or malignancy cannot be determined at CT; type 4=cystic malignant renal tumor. Calcification in a cystic renal mass is not as important in diagnosis as is the presence of associated enhancing septa or mural nodules [35].

The most typical benign renal cystic tumor is multilocular cystic nephroma. Multilocular cystic nephroma is an uncommon benign renal neoplasm composed of multiple, variably sized cysts with prominent septa [33]. The cysts contain non-hemorrhagic fluid and do not communicate with each other. Calcifications are uncommonly present in the cyst wall and septa. In this series, multilocular cystic nephromas (n=5) were characterized by a dense peripheral fibrous capsule. The cysts were lined by cuboidal epithelial cells projecting into the lumen of the cyst. The septal stroma was composed of loose connective tissue with sparse cellularity.

Different malignant renal tumors subtypes which generally reveal a solid pattern may reveal also a cystic pattern. Septal and/or mural nodule contrast enhancement is typically identified in malignant cystic renal tumors and it is determined by the vascular component generated by neoangiogenesis. Papillary cell type RCC may be cystic in the A variant [36] while the clear cell type RCC may be cystic in about the 10% of cases. Cystic clear cell RCC tend to be large, rounded or polylobular lesions [33]. Cystic RCC presents generally a multilocular cystic pattern, with a thick fibrous connective tissue capsule and multiple fibrous septa subdividing the tumor into multiple, variably sized, noncommunicating, fluid-filled loculi. In this series, both cystic clear cells (n=5) and cystic papillary cells type (n=5) RCC revealed septal and/or mural nodules contrast enhancement (Fig. 14).

In some tumors a unilocular pattern may be identified and it is determined by extensive necrosis in a previously solid neoplasm (Fig. 10). The tumoral peripheral wall is thick and irregular and the tumor contains necrotic debris and recent or old hemorrhage. In this series this pattern was identified in one papillary cell type A RCC.

References

1. Pickhardt PJ, Lonergan GJ, Davis CJ, Kashitani N, Wagner BJ (2000) From the archives of AFIP. Infiltrative renal lesions: radiologic–pathologic correlation. Radiographics 20:215–243
2. Levin E, King BF (2000) Adult malignant renal parenchymal neoplasms. In: Pollack HM, McClennan BL, Dyer R (eds) Clinical urography. Saunders, Philadelphia, pp 1440–1470
3. Dalla Palma L, Pozzi Mucelli F, Di Donna A, Pozzi Mucelli R (1990) Cystic renal tumors: US and CT findings. Urol Radiol 12:67–73
4. Storkel S, Eble JN, Adlakha K et al. (1997) Classification of renal cell carcinoma: workgroup no. 1—Union Internationale Contre le Cancer (UICC) and the American Joint Committee on Cancer (AJCC). Cancer 80:987–989
5. Oyen R (1998) Renal Parenchymal tumours. Halley Project 1998–2000, 2nd refresher course series. Springer, Milan, Italy
6. Oyen R, Verswijvel G, Van Poppel H, Roskams T (2001) Primary malignant renal parenchymal epithelial neoplasms. Eur Radiol 11(Suppl 2):S205–S217
7. Pavlovich CP, Schmidt LS, Phillips JL (2003) The genetics basis of renal cell carcinoma. Urol Clin N Am 30:437–454
8. Helenon O, Merran S, Paraf F et al. (1997) Unusual fat-containing tumors of the kidney: a diagnostic dilemma. Radiographics 17:129–144
9. Choyke PL, Glenn GM, Walther MM, Zbar B, Linehan WM (2003) Hereditary renal cancers. Radiology 226:33–46
10. Soyer P, Dufresne AC, Klein I, Barbagelatta M, Herve JM, Scherrer A (1997) Renal cell carcinoma of clear cell type: correlation of CT features with tumor size, architectural patterns and pathologic staging. Eur Radiol 7:224–229
11. Amin MB, Corless CL, Renshaw AA, Tickoo SK, Kubus J, Schultz DS (1997) Papillary (chromophil) renal cell carcinoma: histomorphologic characteristics and evaluation of conventional pathologic prognostic parameters in 62 cases. Am J Surg Pathol 21:621–635
12. Choyke PL, Walther MM, Glenn GM et al. (1997) Imaging features of hereditary papillary renal cancers. J Comput Assist Tomogr 21:737–741
13. Crotty TB, Farrow GM, Lieber MM (1995) Chromophobic cell renal carcinoma: clinicopathologic features of 50 cases. J Urol 154:964–967
14. Jinzaki M, Tanimoto A, Mukai M et al. (2000) Double-phase helical CT of small renal parenchymal neoplasms: correlation with pathologic findings and tumor angiogenesis. J Comput Assist Tomogr 24:835–842
15. Fukuya T, Honda H, Goto K, Ono M et al. (1996) Computed tomographic findings of Bellini duct carcinoma of the kidney. J Comput Assist Tomogr 20:399–403
16. Wagner BJ, Wong You Cheong JJ, Davis CJ (1997) From the archives of the AFIP. Adult renal hamartomas. Radiographics 17:155–169
17. Sherman JL, Hartman DS, Friedman AC et al. (1981) Angiomyolipomas: CT-pathologic correlations of 17 cases. Am J Roentgenol 137:1221–1226
18. Israel G, Bosniak MA (2003) Renal imaging for diagnosis and staging of renal cell carcinoma. Urol Clin N Am 30:499–514
19. Hartman DS (2001) Benign renal and adrenal tumors. Eur Radiol 11(Suppl 2):S195–S204
20. Riccabona M (2003) Imaging of renal tumours in infancy and childhood. Eur Radiol 13(Suppl 4):L116–L129
21. Amin MB, Crotty TB, Tickoo SK, Farrow GM (1997) Renal oncocytoma: a reappraisal of morphologic features with clinicopathologic findings in 80 cases. Am J Surg Pathol 21:1–12
22. Mahnken AH, Günther RW, Tacke J (2004) Radiofrequency ablation of renal tumors. Eur Radiol 14(8):1449–1455

23. Chomas JE, Pollard RE, Sadlowski AR, Griffey SM, Wisner ER, Ferrara KW (2003) Contrast-enhanced US of microcirculation of superficially implanted tumors in rats. Radiology 229:439–446
24. Quaia E, Siracusano S, Bertolotto M et al. (2003) Characterization of renal tumours with pulse inversion harmonic imaging by intermittent high mechanical index technique: initial results. Eur Radiol 13(6):1402–1412
25. Lussanet QG, Backes WH, Griffionen AW et al. (2003) Gadopentetate dimeglumine versus ultrasmall superparamagnetic iron oxide for dynamic contrast-enhanced MR imaging of tumor angiogenesis in human colon carcinoma in mice. Radiology 229:429–438
26. Turetschek K, Huber S, Floyd E et al. (2001) MR imaging characterization of microvessels in experimental breast tumors by using a particulate contrast agent with histopathologic correlation. Radiology 218:562–569
27. van Dijke CT, Brasch RC, Roberts TP et al. (1996) Mammary carcinoma model: correlation of macromolecular contrast-enhanced MR imaging characterizations of tumoral microvasculature and histologic capillary density. Radiology 198:813–818
28. Olsen OE, Jeanes AC, Sebire NJ et al. (2004) Changes in computed tomography features following preoperative chemotherapy for nephroblastoma: relation to histopathological classification. Eur Radiol 14(6):990–994
29. Helenon O, Chretien Y, Paraf F et al. (1993) Renal cell carcinoma containing fat: demonstration with CT. Radiology 188:429–430
30. D'Angelo PC, Gash JR, Horn AW et al. (2002) Fat in renal cell carcinoma that lack associated calcifications. Am J Roentgenol 178:931–932
31. Kido T, Yamashita Y, Sumi S et al. (1997) Chemical shift GRE MRI of renal angiomyolipoma. J Comput Assist Tomogr 21(2):268–270
32. Yoshimitsu K, Honda H, Kuroiuna T et al. (1999) MR detection of cytoplasmic fat in renal cell carcinoma utilizing chemical shift GE imaging. J Magn Reson Imaging 9(4):579–585
33. Hartman DS (ed)(1989) Renal cystic disease. AFIP atlas of radiologic–pathologic correlations. Saunders Company, Philadelphia, USA
34. Bosniak MA (1986) The current radiological approach to renal cyst. Radiology 158:1–10
35. Israel G, Bosniak MA (2003) Calcification in cystic renal masses: is it important in diagnosis? Radiology 226:47–52
36. Roberts SC, Winick AB, Santi MR (1997) Papillary renal cell carcinoma: diagnostic dilemma of a cystic renal mass. Radiographics 17:993–998